

# Voltage fluctuations in ac biased superconducting transition edge sensors.

L. Gottardi,\* M. de Wit, E. Taralli, and K. Nagayashi  
NWO-I/SRON Netherlands Institute for Space Research,  
Sorbonnelaan 2, 3584 CA Utrecht, The Netherlands

A. Kozorezov

Department of Physics, Lancaster University, LA1 4YB, Lancaster, UK

(Dated: October 14, 2022)

We present a detailed analysis of the fundamental noise sources in superconducting transition edge sensors (TESs), ac voltage biased at MHz frequencies and treated as superconducting weak-links. We have studied the noise in the resistive transition as a function of bath temperature of several detectors with different normal resistances and geometries. We show that the ‘excess’ noise, typically observed in the TES electrical bandwidth, can be explained by the equilibrium Johnson noise of the quasiparticles generated within the weak-link. The fluctuations at the Josephson frequency and higher harmonics contribute significantly to the measured voltage noise at the detector bandwidth through the non-linear response of the weak-link with a sinusoidal current-phase relation.

Superconducting transition-edge sensors (TESs) are very sensitive thermometers used as microcalorimeters and bolometers in ground and space-borne low temperature instruments [1, 2]. TESs are, typically, low impedance devices made of a thin superconducting bilayer, with a critical temperature  $T_c$ . They operate in the voltage bias regime. Either a constant or an alternating bias voltage is used, depending on the multiplexing read-out scheme. In the frequency division multiplexing (FDM) configuration considered here, the TES is ac voltage biased in the superconducting transition, by means of high- $Q$   $LC$  resonators at frequencies from 1 up to 5 MHz. The underlying physics of TESs has been extensively studied in the past years and the TES response under ac and dc bias is fairly well described for TESs behaving as superconducting weak-links [3–6], or affected by the generation of phase-slip lines [7].

The basic theory of a TES is extensively reported elsewhere [1, 2, 4]. The electrical and thermal equations for a TES are solved exactly in the small signal regime with resistance dependency on temperature  $T$  and current  $I$  linearly expanded to the first-order as  $R(I, T) = R_0 + \alpha \frac{R_0}{T_0} \delta T + \beta \frac{R_0}{I_0} \delta I$ . Here,  $\alpha = (T/R)(\partial R/\partial T)|_{I_0}$ ,  $\beta = (I/R)(\partial R/\partial I)|_{T_0}$ ,  $\delta T = T - T_0$  and  $\delta I = I - I_0$ . The  $\alpha$  and  $\beta$  parameters can be measured experimentally at the operating point and are used to estimate the detector noise and sensitivity. Three fundamental contributions to the TES noise are generally identified. The first one is called *phonon noise* from thermal fluctuations between the TES-absorber body and the heat bath, with power spectral density given by  $S_{ph} = 4k_B T^2 G_{bath} ((T_{bath}/T)^{n+2} + 1)/2$ , where  $G_{bath}$  is the thermal conductance to the bath at a temperature  $T_{bath}$  and  $n$  is the exponent depending on the nature of thermal processes involved. This noise is dominant at

low frequencies in the detector thermal bandwidth typically below  $\sim 200$ Hz. The second contribution is the *Johnson-Nyquist noise* (JN) of the TES biased in the resistive transition. It has been modelled so far as a non-equilibrium Johnson noise (NEJN) with voltage spectral density  $S_{V,nejn} = 4k_B T \text{Re}(Z_{tes})(1 + 2\beta)$  [8]. It is suppressed at low frequency by the electro-thermal feedback [9] and becomes significant in the detector electrical band at kHz. The third noise term is the *internal thermal fluctuation noise* (ITFN), which is generated by thermal fluctuation between distributed heat capacities internal to the TES-absorber system. It has a power spectral density  $S_{itfn} = 4k_B T^2 G_{tes}$ , where  $G_{tes}$  is the intrinsic thermal conductance of the system. The response of the detector to this noise source is identical to the JN noise, which complicates the identification of the TES noise sources in the electrical bandwidth. The ITFN can be derived from a proper characterization of the thermal circuit [10–14]. In Fig. (1), we show the typical current noise spectrum after demodulation of a MHz biased TES operating at  $R/R_N = 20\%$ , where  $R_N$  is the TES normal resistance. More details on how to derive the total current noise measured in a TES from the noise sources described above is given in the supplemental material [15]. So far, the total TES noise in the JN bandwidth has not been fully understood. The residual  $M^2 = (S_{V,data} - S_{V,model})/S_{V,model}$  is a convenient way to characterize the ‘excess’ noise. The common practice in the TES literature is to define  $M^2$  with respect to the NEJN, i.e.  $S_{V,model} = S_{V,nejn}$  [4, 11, 14, 18].

In this Letter, we study the Johnson-Nyquist (JN) noise in many ac biased TESs with different electro-thermal properties. We show that the fluctuation-dissipation theorem generalized for a non-linear system in thermal equilibrium explains well the observed noise and that it is not necessary to introduce the formalism for a non-linear TES out-of-equilibrium [8]. The observed spectral density of fluctuations of the TES voltage is in full agree-

\* Electronic mail: l.gottardi@sron.nl

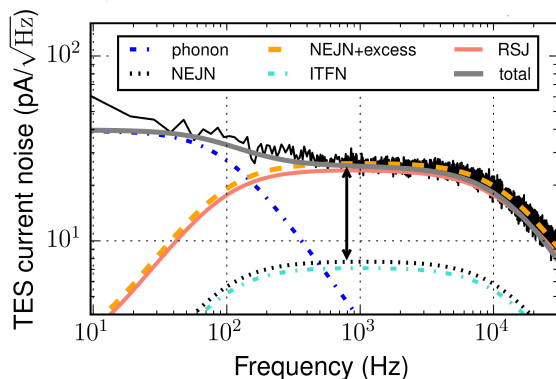


FIG. 1. Current noise spectrum for a TiAu  $80 \times 20 \mu\text{m}^2$  TES biased at 2.6 MHz,  $R/R_N = 13\%$  and  $T_{\text{bath}} = 55 \text{ mK}$ . The different lines show the noise contributions discussed in the text. The vertical arrow indicates the measured excess noise with respect to the estimated NEJN.

ment with the expected equilibrium thermal noise of the quasi-particles. We characterized, at different bias frequencies, many Ti/Au TES microcalorimeters, with critical temperature  $T_c \sim 90 \text{ mK}$ , normal sheet resistance  $R_{\square} = 26 \text{ m}\Omega/\square$  and three different geometries (length  $\times$  width):  $80 \times 40$ ,  $80 \times 20$  and  $120 \times 20 \mu\text{m}^2$ , leading to different values of  $R_N$ ,  $\alpha$ ,  $\beta$ , and saturation power. In this way we can probe the noise model in different weak-link regimes [19]. More details on the devices and the read-out system are given in [15, 19]. To study the intrinsic fluctuations inside the TES, we consider the seminal work of Likharev and Semenov [20] and later reviews [21, 22]. We consider the RSJ model previously proposed to explain the excess noise in dc-biased TES [23], extend it to the ac bias case and provide experimental evidence of its validity. Moreover, as proposed in [24, 25], we compare the RSJ approximation with the generalized kinetic theory for fluctuations in superconductors derived by Kogan and Nagaev (KN) [26] and show that the two models are consistent with each other over a wide range of bias conditions, detector  $\beta$  values and for different TES geometries. In [25], only the results for two dc biased TESs are reported and a relatively large discrepancy between the two models is observed. Following the method described in this letter, the detector noise is accurately estimated since we measure directly the physical quantities required by the RSJ and KN models and no free parameters are left. A fundamental difference between a dc and ac biased TES is given by the evolution of the superconducting phase across the  $SS'S$  or  $SNS$  weak-link. Under dc bias, due to the ac Josephson effect, the phase  $\varphi(t)$  increases linearly with time at a rate  $\omega_J = 2eV_{\text{dc}}/\hbar$  proportional to the bias voltage, where  $\omega_J$  is the bias dependent Josephson frequency. Under ac bias, on the contrary,  $\varphi(t)$  oscillates around an equilibrium value  $\varphi_0$  at a frequency  $\omega_J = \omega_b$ , out-of-phase with respect to the

ac bias voltage  $V(t) = V_{\text{ac}} \cos(\omega_b t)$ , and with a peak amplitude  $\varphi_{pk} = 2eV_{\text{ac}}/\hbar\omega_b$ . Despite the difference, when studying the voltage fluctuations within the weak-link context, both the dc and ac biased TES can be seen as a periodical non-stationary system with period  $2\pi/\omega_J$ . It is then convenient to represent the time dependent system as a combination of Fourier series over frequencies  $\omega_m = \omega + m\omega_J$  and solve the problem of the weak-link dynamics as done by Zorin [21, 27]. It is shown that the voltage power spectral density of the fluctuation  $S_V(\omega)$  is the results of parametric conversion of fluctuations mixed with the Josephson oscillations and its harmonics. The relation with the current power spectrum  $S_I(\omega)$  is given by  $S_V(\omega) = \sum Z_{mm'}^*(\omega) Z_{mm'}(\omega) S_I(\omega_m)$ . Here,  $Z_{mm'}(\omega)$  is the impedance matrix of the RSJ, with the indices  $m$  and  $m'$  standing for the respective harmonics of the Josephson oscillation at  $\omega_J$  [20, 21]. When measuring the noise at  $\omega \ll \omega_J$ , the contribution from the higher harmonics with  $|m| > 1$  was shown to be negligible [28]. The low frequency power spectral density of the voltage fluctuations, averaged over the period of oscillation  $2\pi/\omega_J$  for an RSJ can be approximated [15, 21, 23, 29] to

$$S_V(\omega) \simeq R_d^2 \left[ \frac{3}{2} \frac{R}{R_N} \left( 1 - \frac{1}{3} \left( \frac{R}{R_N} \right)^2 \right) \right] S_I(\omega), \quad (1)$$

where  $R_d = \partial V / \partial I = R(1 + \beta)$  is the detector dynamic resistance at the bias point. The Eq. (1) is valid both for a dc and an ac biased TES [15].

A more general derivation of the spectral density of the voltage fluctuation for a resistively shunted Josephson contact, with arbitrary current-phase relation  $I(\varphi)$ , has been derived by Nagaev [30]. The calculation is done for a junction biased at a current  $I > I_c$  in the region where the quasiparticle distribution function is close to equilibrium and the correlation function of the current is determined by the JN formula. The spectral density  $S_V(\omega)$  at frequency  $\omega < \omega_J$  is equal to

$$S_V(\omega) = R_d^2 \left[ 1 - \frac{\hat{V}}{2R_d^2} \frac{\partial R_d}{\partial I} \right] S_I(\omega). \quad (2)$$

The two terms in the bracket describe the noise of the thermal fluctuations at equilibrium and should be experimentally compared with Eq. (1) derived for an RSJ with sinusoidal current-phase relation. In the derivation of Eq. (1) and Eq. (2), the system is considered to be in thermodynamic equilibrium and the fluctuation-dissipation theorem applies for the thermally excited quasiparticles [31] so that  $S_I(\omega) = 4k_B T / \text{Re}(Z_{\text{tes}}(\omega))$ , i.e. the TES JN is treated as equilibrium thermal noise with the non-linearity given by the Josephson impedance  $Z_{mm}$ .

The TES electrical noise can be calculated rather precisely from Eq. (1) and Eq. (2) at each bias point after estimating the detector electro-thermal parameters.

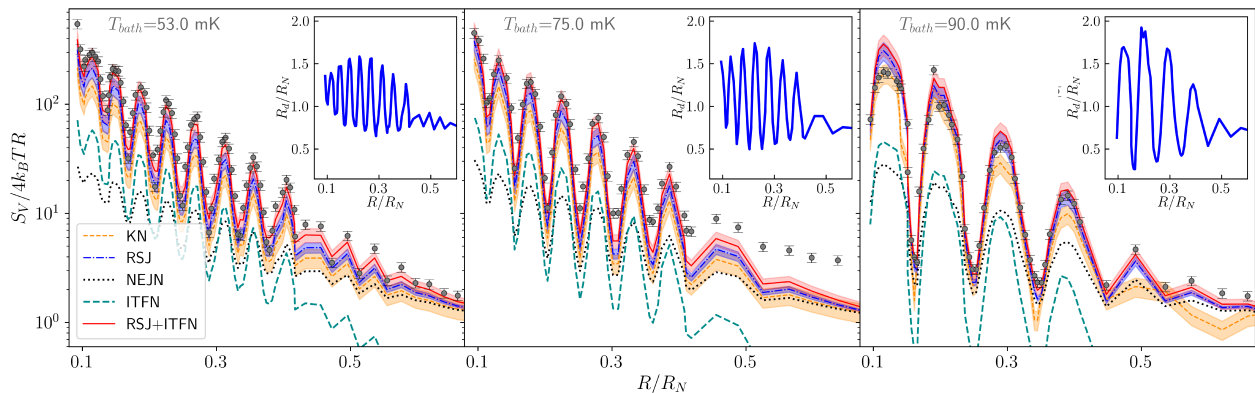


FIG. 2. Measured voltage noise of the  $80 \times 40 \mu\text{m}$  TES as a function of bias point  $R/R_N$ . From top to bottom:  $T_{\text{bath}} = 53.0, 75.0$  and  $90.0$  mK. The blue dot-dashed and the orange dashed lines are the prediction from Eq. (1) and Eq. (2), respectively. The green dashed line is the estimated ITFN. The black dotted line is the NEJN. The red line is the sum in quadrature of the RSJ and ITFN noise. Insets: the normalized TES dynamic resistance,  $R_d = R(1 + \beta)$  as a function of  $R/R_N$ .

This is done by evaluating the TES complex impedance  $Z_{tes}(\omega, I_0, T_0)$  using the standard technique of measuring the detector current response to a voltage excitation at a given frequency  $\omega$ . The formalism for a dc and ac biased TES has been described in [32] and [33], respectively. The classical expression for  $Z_{tes}(\omega)$  [32] has been modified in [34] to include the intrinsic reactance predicted by the RSJ model. The details are reviewed in [15].

The theoretical predictions described above can be verified experimentally. By fitting the complex impedance curves taken along the transition, as described in [15], we estimate the TES linear parameters  $\alpha$ ,  $\beta$  and the detector time constants for many devices and bias frequencies. From  $\beta$  and  $R_d = R(1 + \beta)$ , we calculate for each bias point the total TES voltage spectral density as in Eq. (1). Evaluating the JN from Eq. (2) requires the derivative of the dynamic resistance with respect to the current, which cannot be accurately obtained from the  $I - V$  characteristic.

Our technique of measuring  $Z_{tes}$  provides a straightforward estimation of  $R_d$  and  $\partial R_d / \partial I$ . We use the fact that  $\partial R_d / \partial I = -R_d^3 \partial^2 I / \partial V^2$ , and that the TES current response to a small and slow modulation  $V_m \cos \omega t$  of the voltage bias, with  $V_m \ll V_{ac}$  and  $\omega \ll \omega_b$ , can be expanded as

$$I(V, t) = I(V) + \frac{\partial I}{\partial V} V_m \cos \omega t + \frac{1}{2} \frac{\partial^2 I}{\partial V^2} V_m^2 \cos^2 \omega t + \dots \quad (3)$$

The first harmonic is proportional to the inverse of the dynamic resistance  $\partial I / \partial V = 1/R_d$ , while the second harmonic gives the term  $\partial^2 I / \partial V^2$ , which is needed to estimate the noise as in Eq. (2). When measuring the intrinsic complex impedance curves, we fit the sinusoidal response up to the third order, to capture the harmonic distortions generated by the Josephson non-linearity as a function of bias point. An example of the fit of the response to a sinusoidal excitation is shown in [15]. The

coefficient of the first and second order term of the fit is used to accurately estimate the noise from the KN derivation.

We measured the noise for many pixels along the TES resistive transitions. A typical data set is shown in Fig. (2) for a  $80 \times 40 \mu\text{m}$  TES biased at 2.5 MHz. The voltage noise, measured in the kHz bandwidth, normalised to the thermal noise of resistance  $R = \text{Re}(Z_{tes}(\omega))$ , is plotted as a function of  $R/R_N$ , along with the different noise contributions. The noise shows the expected oscillating behaviour from the Josephson effects being strongly correlated with the TES dynamic resistance. The first main result is that the NEJN dramatically underestimates the noise, in particular at low  $R/R_N$  values. The total observed noise is consistent with the prediction from Eq. (1) or Eq. (2), within the  $1\sigma$  experimental uncertainties indicated by the shaded area around the lines. This result is in agreement with the fluctuation-dissipation theorem generalized for a non-linear system in thermal equilibrium. The major contribution to the error bars derives from the uncertainties in the estimation of the bias circuit parameters, known within 10%, which propagate in the calculation of  $V_{tes}$ ,  $P_{tes}$ ,  $G_{bath}$ ,  $\alpha$  and  $\beta$ . The second important result is that both the RSJ model and the derivation from KN explain equally well the detector noise. This implies that the sinusoidal current-phase relation assumed in the RSJ model is a good approximation for the detectors and bias conditions discussed here. This is expected when a TES is treated as an SNS long diffusive weak-link with Thouless energy  $E_{TH} = \hbar D / L^2$ , where  $D \simeq 0.018 \text{ m}^2/\text{s}$  is the diffusion coefficient for Au and  $L = 80 - 120 \mu\text{m}$  the TES length, satisfying the condition  $E_{TH} \ll eV \ll k_B T$ . The contribution of the ITFN noise for this particular design is typically small, and accounts for about 20% of the total noise. The ITFN is estimated from the Wiedemann-Franz law with  $G_{tes} = L_0 T / R_{\square}$ , where  $L_0$  is the Lorenz number

[35]. Some excess noise is observed at  $R/R_N > 0.4$  for  $T_b = 55$  and  $75$  mK, and it will be discussed later below.

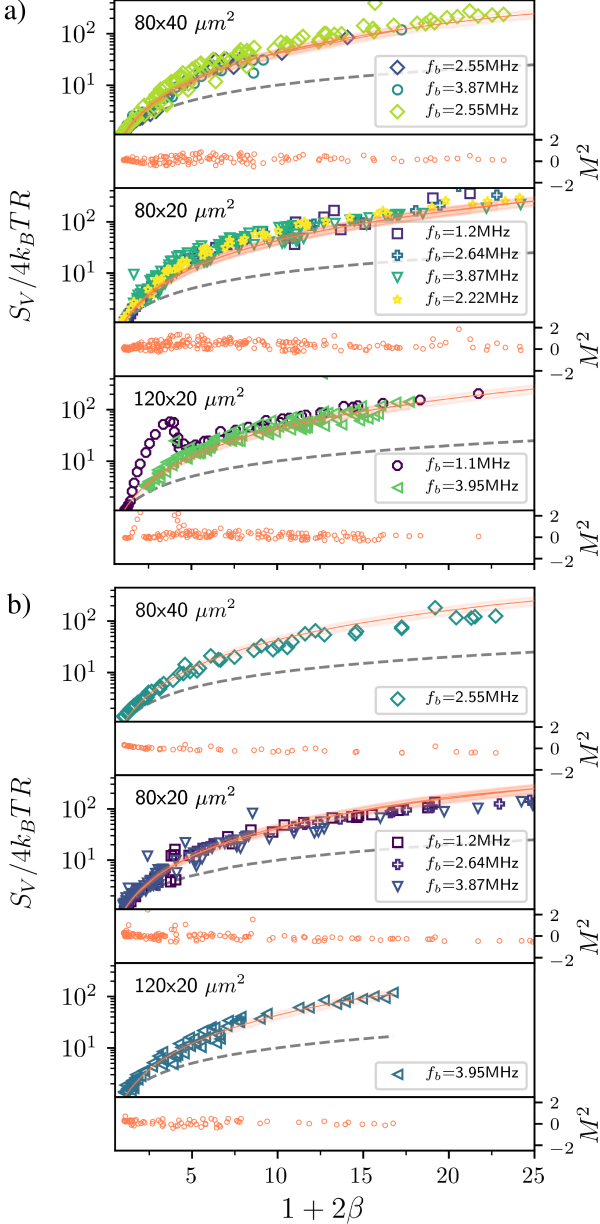


FIG. 3. Voltage noise, after ITFN subtraction, for three different TES design and several bias frequencies, measured at  $T_{bath} = 53$  mK(a) and  $T_{bath} = 90$  mK(b), respectively. The dashed line shows the noise estimation from NEJN. The red solid line is the prediction from the RSJ noise, with the shaded area indicating the  $1\sigma$  uncertainty on the calculated noise. The red open circle is the residual  $M^2$  calculated with respect to the RSJ model for all the measured pixels.

To our knowledge, this is for the first time that the general derivation proposed by Nagaev [30] has been experimentally compared against the RSJ prediction. Eq. (2) was used before [24] to explain the shot noise in the co-

herent regime of long diffusive SNS junctions at low bias voltage,  $eV < E_{TH}$ . In Fig. (3), we summarise the noise measurement done for many other pixels with the three different TES geometries, biased at frequencies from 1.1 to 3.95 MHz. We plot the voltage noise as a function of the factor  $1 + 2\beta$  (derived for the NEJN [8]), after subtracting the ITFN contribution. The solid red line is the expected RSJ noise with the shaded area highlighting the  $1\sigma$  uncertainties. The dashed line is the calculated NEJN. As shown by the small residual  $M^2$  calculated using the RSJ model, the TES JN is in very good agreement with the RSJ prediction over a large range of  $\beta$  and for the high and low TES power regime ( $T_{bath} = 53$  and  $90$  mK, respectively). The measured and expected noise is generally independent on the bias frequency. Excess noise is observed at low value of  $\beta$  ( $\lesssim 3$ ) with some pixels (for example the  $120 \times 20 \mu\text{m}^2$  biased at 1.1 MHz, and few  $80 \times 20 \mu\text{m}^2$  pixels at a  $T_{bath} = 53$  mK [Fig. (3)(a)]. Fig. (4) shows the details of the observed excess noise for two devices as a function of  $R/R_N$  and  $T_{bath}$ . This

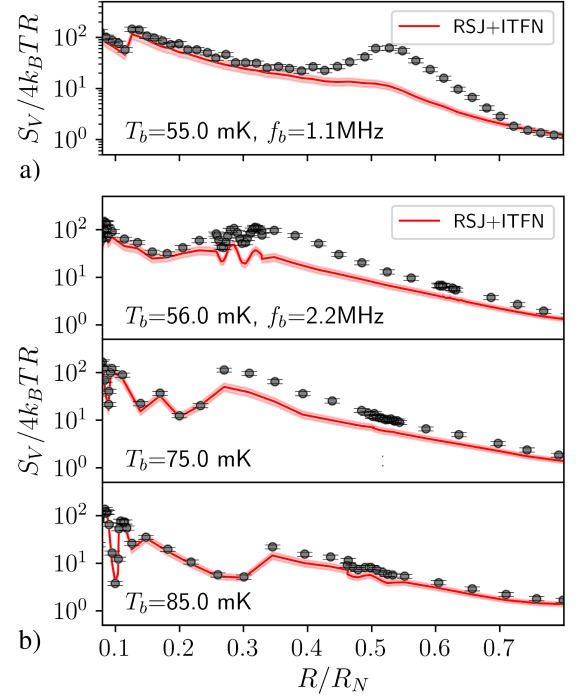


FIG. 4. Measured voltage noise at  $T_{bath} = 55.0$  mK of two  $120 \times 20 \mu\text{m}$  TES as a function of bias point  $R/R_N$  biased respectively at (a) 1.1 and (b) 2.2 MHz. The latter was measured at (from top to bottom)  $T_{bath} = 56.0, 75.0$  and  $85.0$  mK. The red curve is the expected RSJ and ITFN noise.

noise is reduced when operating the device close to  $T_c$ , i.e. at lower TES current [15]. We believe this noise is of a different nature than the noise discussed above, which depends on the TES  $R$ ,  $\beta$  and  $T$  and not on the current (Eq. (1)). It is likely due to a non-uniform current and temperature distribution inside the TES caused by the

presence of normal metal structures (the stems connecting the absorber [15]) in the current path. The effect is minimized when operating the device close to  $T_c$ . From a recent investigation it seems possible to eliminate the excess noise bumps by optimizing the size and the position of the absorber-TES stems. A full study is under way.

In conclusion, we have extensively characterized at MHz bias the voltage fluctuations of TES microcalorimeters with three different design and  $R_N$ . When subtracting the expected ITFN noise, the residual noise in the JN bandwidth can be well explained, over a large range of experimental parameters ( $R_N, V_{tes}, f_b, T_{bath}$ ), from the theory of noise in Josephson weak-links, following the RSJ model or the more general derivation from KN [26]. The noise is consistent with the equilibrium thermal noise and is enhanced by the non-linear response of the weak-link.

This work is partly funded by European Space Agency (ESA) under ESA CTP contract ITT AO/1-7947/14/NL/BW, by the European Union's Horizon 2020 Program under the AHEAD project (Grant Agreement Number 654215) and is part of the research program Athena (project number 184.034.002), which is (partly) financed by the Dutch Research Council (NWO).

- 
- [1] K. D. Irwin and G. C. Hilton, *Cryogenic Particle Detection* (Springer-Verlag, 2005) p. 63–149.
- [2] J. N. Ullom and D. A. Bennett, *Supercond. Sci. Technol.* **28**, 084003 (2015).
- [3] J. E. Sadleir, S. J. Smith, S. R. Bandler, J. A. Chervenak, and J. R. Clem, *Phys. Rev. Lett.* **104**, 047003 (2010).
- [4] S. J. Smith, J. Adams, C. Bailey, S. R. Bandler, J. A. Chervenak, M. Eckart, F. Finkbeiner, R. Kelley, C. Kilbourne, F. Porter, and J. Sadleir, *J. Appl. Phys.* **114**, 074513 (2013).
- [5] L. Gottardi, S. J. Smith, A. Kozorezov, H. Akamatsu, J. van der Kuur, S. R. Bandler, M. P. Bruijn, J. A. Chervenak, *et al.*, *J. Low Temp. Phys.* **193**, 209 (2018).
- [6] L. Gottardi, A. Kozorezov, H. Akamatsu, J. van der Kuur, M. P. Bruijn, R. H. den Hartog, R. Hijmering, P. Khosropanah, C. Lambert, A. J. van der Linden, M. L. Ridder, T. Suzuki, and J. R. Gao, *Appl. Phys. Lett.* **105**, 162605 (2014).
- [7] D. A. Bennett, D. S. Swetz, D. R. Schmidt, and J. N. Ullom, *Phys. Rev. B* **87**, 020508(R) (2013).
- [8] K. Irwin, *Nucl. Instrum. and Methods Phys. Res. Sect. A* **559**, 718 (2006).
- [9] K. D. Irwin, *Appl. Phys. Lett.* **66**, 1998 (1995).
- [10] H. F. C. Hoevers, A. C. Bento, M. P. Bruijn, L. Gottardi, M. A. N. Korevaar, W. A. Mels, and P. A. J. de Korte, *Appl. Phys. Lett.* **77**, 4422 (2000).
- [11] Y. Takei, L. Gottardi, H. Hoevers, A. J. de Korte, J. van der Kuur, M. L. Ridder, and M. P. Bruijn, *J. Low Temp. Phys.* **151**, 161 (2008).
- [12] K. M. Kinnunen, M. R. J. Palosaari, and I. J. Maasilta, *J. Appl. Phys.* **112**, 034515 (2012).
- [13] I. J. Maasilta, *AIP Advances* **2**, 042110 (2012).
- [14] N. A. Wakeham, J. S. Adams, S. R. Bandler, S. Beaumont, J. A. Chervenak, A. M. Datesman, M. E. Eckart, F. M. Finkbeiner, R. Hummatov, R. L. Kelley, C. A. Kilbourne, A. R. Miniussi, F. S. Porter, J. E. Sadleir, K. Sakai, S. J. Smith, and E. J. Wassell, *J. Appl. Phys.* **125**, 164503 (2019); *J. Low Temp. Phys.* **200**, 192 (2020).
- [15] See Supplemental Material at [URL will be inserted by publisher].
- [16] J. Ullom, W. Doriese, G. Hilton, J. Beall, S. Deiker, K. Irwin, C. Reintsema, L. Vale, and Y. Xu, *Nucl. Instrum. Methods A* **520**, 333 (2004).
- [17] M. de Wit, L. Gottardi, E. Taralli, K. Nagayoshi, M. L. Ridder, H. Akamatsu, M. P. Bruijn, M. D'Andrea, J. van der Kuur, K. Ravensberg, D. Vaccaro, S. Visser, J. R. Gao, and J.-W. A. den Herder, *J. Appl. Phys.* **128**, 224501 (2020).
- [18] K. Likharev and V. Semenow, *Sov. Phys. JEPT Lett* **15**, 442 (1972).
- [19] S. Kogan, *Electronic Noise and Fluctuations in Solids*, 1st ed. (Cambridge University Press, USA, 2008).
- [20] A. Vystavkin, V. Gubankov, L. Kuzmin, K. Likharev, V. Migulin, and V. Semenov, *Rev. Phys. Appl.* **9**, 79 (1974).
- [21] A. Kozorezov, A. Golubov, D. Martin, P. de Korte, M. Lindeman, R. Hijmering, J. van der Kuur, H. Hoevers, L. Gottardi, M. Kupriyanov, and J. Wigmore, *J. Low Temp. Phys.* **167**, 108 (2012).
- [22] E. Lhotel, O. Coupiac, F. Lefloch, H. Courtois, and M. Sanquer, *Phys. Rev. Lett.* **99**, 117002 (2007).
- [23] A. Wessels, K. Morgan, D. T. Becker, J. D. Gard, G. C. Hilton, J. A. B. Mates, C. D. Reintsema, D. R. Schmidt, D. S. Swetz, J. N. Ullom, L. R. Vale, and D. A. Bennett, arXiv:1907.11343 (2019).
- [24] S. M. Kogan and K. Nagaev, *Zh. Eksp. Teor. Fiz* **94**, 262 (1988).
- [25] A. B. Zorin, *Physica B+C* **108**, 1293 (1981).
- [26] R. H. Koch, D. J. Van Harlingen, and J. Clarke, *Phys. Rev. B* **26**, 74 (1982).
- [27] L. G. Aslamazov and A. I. Larkin, *SJETP Lett.* **9** (1969).
- [28] K. E. Nagaev, *Sov. Phys. JETP* **67**, 579 (1988), and arXiv:1911.09941 [cond-mat.mes-hall].
- [29] D. Rogovin and D. Scalapino, *Ann. of Phys.* **86**, 1 (1974).
- [30] M. A. Lindeman, S. Bandler, R. P. Brekosky, J. A. Chervenak, E. Figueroa-Feliciano, F. M. Finkbeiner, M. J. Li, and C. A. Kilbourne, *Rev. Sci. Instrum.* **75**, 1283 (2004).
- [31] E. Taralli, P. Khosropanah, L. Gottardi, K. Nagayoshi, M. L. Ridder, M. P. Bruijn, and J. R. Gao, *AIP Advances* **9**, 045324 (2019).
- [32] A. Kozorezov, A. A. Golubov, D. Martin, P. de Korte, M. Lindeman, R. Hijmering, J. van der Kuur, H. Hoevers, L. Gottardi, M. Kupriyanov, and J. Wigmore, *Appl. Phys. Lett.* **99**, 063503 (2011).
- [33] The internal thermal conductance in a long SNS junction is not trivial to calculate and it is likely changing along the transition. Assuming that  $G_{WF}$  depends on  $R_{\square}$  gives typically the best noise estimation over the whole transition in our TESs. The noise, in particular at low TES resistance biasing, turns out to be overestimated when  $G_{WF}$  is calculated using  $R_N$  as in [14].
- [34] C. Kirsch, L. Gottardi, M. Lorenz, T. Dauser, R. den Hartog, B. Jackson, P. Peille, S. Smith, and J. Wilms, *J. Low Temp. Phys.* **199**, 569 (2020).
- [35] W.T. Coffey, J.L. DeJardin, and Y.P. Kalmykov, *Phys. Rev. B* **62**, 3480 (2000).

## Supplemental Materials: Voltage Fluctuations in ac Biased Superconducting Transition-Edge Sensors.

### THE ELECTRO-THERMAL CIRCUIT AND THE DERIVATION OF THE COMPLEX IMPEDANCE AND THE NOISE OF A TES BEHAVING AS A WEAK-LINK

We have characterized many Ti/Au TES microcalorimeters at different bias frequencies. The TESs have a critical temperature  $T_c \sim 90$  mK, normal sheet resistance  $R_{\square} = 26$  m $\Omega/\square$  and geometry  $L \times W = 80 \times 40$ ,  $80 \times 20$  and  $120 \times 20$   $\mu\text{m}^2$ . A schematic diagram of the measured devices is shown in Fig. (S1)(a). The normal resistance of the

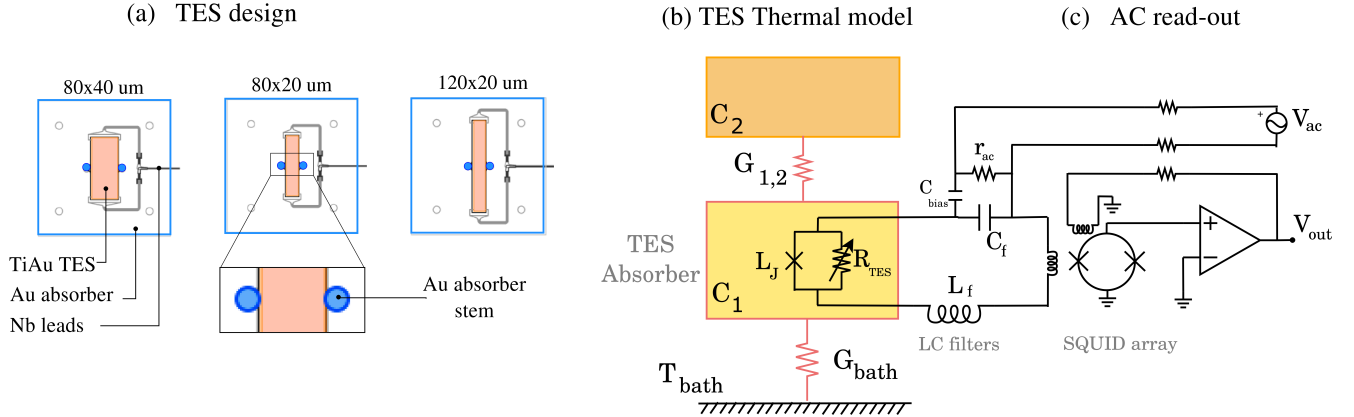


FIG. S1. (a) Schematic diagram of the Ti/Au TESs studied in this work. Their geometry is, respectively,  $80 \times 40$ ,  $80 \times 20$  and  $120 \times 20$   $\mu\text{m}^2$ , which correspond to an aspect ratio  $L/W = 2, 4$  and  $6$ . The TESs are connected to a  $2.3$   $\mu\text{m}$  thick,  $240 \times 240$   $\mu\text{m}^2$ , Au absorber via the two central stems. The stems are in Au and have a diameter of  $10$   $\mu\text{m}$ . (b) a two-body thermal model of the TES calorimeter. (c) The MHz bias and read-out electrical circuit used in the experiment. The detector is ac voltage biased in the superconducting transition, by means of a high- $Q$   $LC$  resonator at frequency from  $1$  up to  $5$  MHz. The TES current is measured by an array of SQUIDs amplifier.

three TES design is,  $R_N = 52, 104$  and  $156$  m $\Omega$  and the measured thermal conductance-to-bath is  $G_{bath} = 110, 80$  and  $110$  pW/K, respectively. The TESs are thermally coupled to a  $2.3$   $\mu\text{m}$  thick,  $240 \times 240$   $\mu\text{m}^2$  large Au absorbers by means of two Au stems,  $10$   $\mu\text{m}$  in diameter, in the middle of the TES bilayer. The detectors are suspended on  $0.5$   $\mu\text{m}$  SiN membranes. More details on the electro-thermal properties of these devices can be found in [19]. The TES-absorber system is thermally described with a two-body model schematically reported in Fig. (S1)(b). In line with the results from [14], we believe the TES bilayer itself has a limited thermal conductance  $G_{12}$  and  $C_2$  is a fraction of the TES heat capacitance  $C_{tes}$ .  $C_1 = C_{tes} + C_{abs}$ , where  $C_{abs}$  is the heat capacitance of the absorber. For our devices  $C_{abs} \gg C_{tes} - C_2 > C_2$ .

The read-out scheme is shown in Fig. (S1)(c). The detector is ac voltage biased in the superconducting transition, by means of a high- $Q$   $LC$  resonator at frequency from  $1$  up to  $5$  MHz, and works as amplitude modulator. The MHz signal is amplified by an array of Superconducting QUantum Interference Devices and demodulated at room temperature. After demodulation, the signal can be treated as in the dc bias case.

The linearized system of the electrical and thermal differential equations are reported here in the frequency space and matrix form:

$$\underbrace{\begin{pmatrix} z_{th}(\omega) + R(1 + \beta) + dZ_{wl} & \mathcal{L}_0 G_{bath}/I & 0 \\ -(2 + \beta)IR - 2IdZ_{wl} & G_{bath}(1 - \mathcal{L}_0) + G_{12} + i\omega C_1 & -G_{12} \\ 0 & -G_{12} & +G_{12} + i\omega C_2 \end{pmatrix}}_{\mathcal{M}} \begin{pmatrix} \Delta I(\omega) \\ \Delta T_1(\omega) \\ \Delta T_2(\omega) \end{pmatrix} = \begin{pmatrix} v_{jn} \\ p_{ph} - Iv_{jn} \\ p_2 \end{pmatrix} = \sqrt{S_{vp}}, \quad (S1)$$

where  $z_{th}(\omega)$  is the Thevenin equivalent of the bias circuit in Fig. (S1),  $\mathcal{L}_0 = I^2 R \alpha / G_{bath}$  is the zero frequency the electrothermal feedback loop gain [1, 32] and  $dZ_{wl}$  is the correction term to the TES impedance from the RSJ model as it is derived below. The noise terms,  $\sqrt{S_{vp}}$  on the right-hand side of the equation are the detector voltage and power noise sources described in the main text, with:  $v_{jn} = \sqrt{S_{V,model}}$  the Johnson-Nyquist noise term, the main

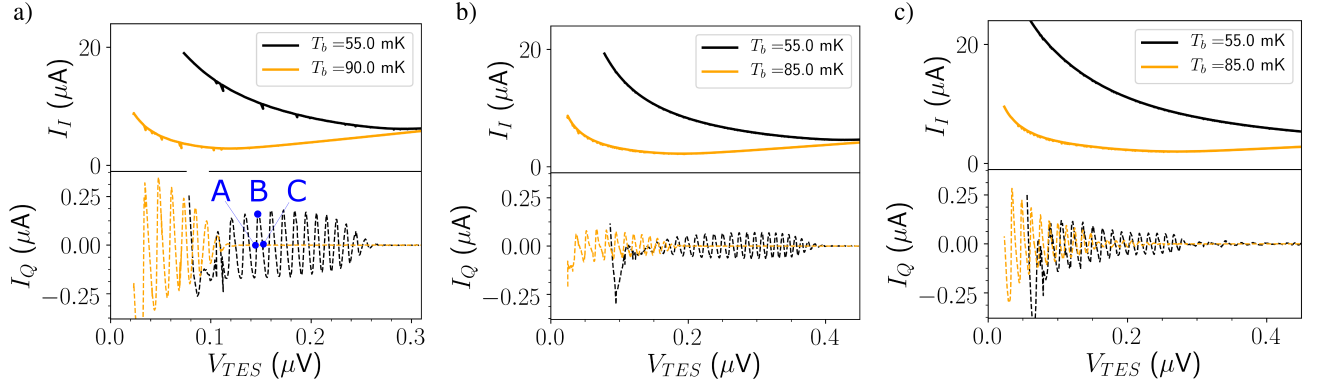


FIG. S2. In-phase,  $I_I$ , and quadrature,  $I_Q$ , TES current vs voltage, for the three TES geometries,  $80 \times 40$  (a),  $80 \times 20$  (b) and  $120 \times 20$  (c)  $\mu\text{m}^2$ , all biased at  $f_b = 2.5$  MHz. The  $I_I, I_Q - V$  curves at  $T_{\text{bath}} = 55$  mK (black lines), and 90 mK(a) and 85 mK(b,c) (orange lines) are shown. In (a), the A,B and C are the bias points discussed in Fig. (S3) and in the related text. In colors on line.

topic of our manuscript,  $p_{ph} = \sqrt{S_{ph}}$  the phonon noise and  $p_2 = \sqrt{S_{itfn}}$  the ITFN noise. The total TES current noise, plotted in Fig.(1) of the main text, is obtained from  $i_{n,tes} = \sqrt{(\mathcal{M}\mathcal{M}^*)^{-1}S_{vp}}$ .

In Fig. (S2), we show the in-phase (solid line),  $I_I$ , and quadrature (dashed line),  $I_Q$ , for the three TES microcalorimeter geometries. They represent respectively the *quasiparticles* and the *supercurrent* as described by the Josephson equations. The IV curves were measured at  $T_{\text{bath}} = 55$  mK (black) and 85, 90 mK (orange), with the detectors biased at  $\sim 2.5$  MHz. The period and amplitude of oscillation of the supercurrent as a function of the TES voltage can be described within the theoretical framework based on the resistively shunted junction model (RSJ) [34], extended to calculate the stationary non-linear response of a TES to a large ac bias current in the presence of noise [6, 16]. The TES quiescent temperature  $T$  is calculated from the  $I_I - V$  characteristics and the detector power low,  $P = I_I V = k(T^n - T_{\text{bath}}^n)$ , where  $k = G_{\text{bath}}/n(T^{n-1})$ .  $G_{\text{bath}}$  is estimated by taking many  $I - V$  curves at different bath temperature  $T_{\text{bath}}$  and by fitting the  $P - T_{\text{bath}}$  curve [19].

In the main text, we have shown that the voltage power spectral density of the fluctuation  $S_V(\omega)$  is the results of parametric conversion of fluctuations mixed with the Josephson oscillations and its harmonics. Within the RSJ model, the low frequency power spectral density of the voltage fluctuations across the weak-link, averaged over the period of oscillation  $2\pi/\omega_J$ , is

$$S_V(\omega) = R_d^2 \left[ 1 + \frac{1}{2x^2} \right] S_I(\omega), \quad (\text{S2})$$

where  $R_d = \partial V / \partial I = R(1 + \beta)$  is the detector dynamic resistance at the bias point, and  $x = I/I_c(T)$ , with  $I$  and  $I_c(T)$  the TES current and Josephson critical current respectively. To derive Eq. (S2) we have used the following relations, which are valid for a RSJ with thermal energy  $k_B T$  larger than  $\hbar\omega_J$  and for  $\omega \ll \omega_J$  [20, 21]:  $|Z_{00}(\omega)| = R_d$ ,  $|Z_{01}(\omega)| = |Z_{0-1}(\omega)| = \frac{1}{2x} |Z_{00}|$  and  $S_I(\omega_J) = S_I(\omega)$ . We have not considered quantum correction since, for a typical TES,  $k_B T \gg eV$ . The Eq. (S2) is valid both for a dc and ac biased TES. We can approximate Eq. (S2) using the solution of the Josephson equations [29] in the RSJ model, valid for  $I > I_c$ . The current-voltage characteristic, averaged over a period of oscillations,  $2\pi/\omega_J$ , becomes then  $\hat{V} = I_c R_N \sqrt{x^2 - 1}$ , with  $R_N$  the resistance of the weak-link in the normal state. From the definition of the dynamic resistance, and with  $R = \text{Re}(Z_{tes})$ , it can be shown [21, 23] that  $1/2x^2 = 1/2 [1 - (R_N/R)^2/(1 + \beta)^2]$ , which, from Eq. (S2), leads to Eq. (1) of the main text.

The classical expression for the TES complex impedance  $Z_{tes}(\omega)$  [1, 32] has been modified by including the intrinsic reactance predicted by the RSJ model. From the results in [34] and the discussion reported in [22, 27], the expression for  $Z_{tes}(\omega)$ , for a TES ac biased at a frequency  $\omega_b$ , becomes:

$$Z_{tes}(\omega) = Z_{tes}^0(\omega) + dZ_{wl}(\omega) = Z_{tes}^0(\omega) + \frac{1}{1 - \mathcal{L}_0} \frac{Z_{00}(\omega + \omega_b) - Z_{00}(\omega_b)}{1 - i\omega\tau_{eff}}, \quad (\text{S3})$$

where  $Z_{tes}^0(\omega)$  is the classical TES impedance, which, for the two-body model described before, takes the form

$$Z_{tes}^0(\omega) = R \left[ 1 + \beta + \frac{(2 + \beta)\mathcal{L}_0}{i\omega\tau_{01} - \mathcal{L}_0 + 1 - G_{12}/(G_1 + G_2)} \frac{1}{1 + i\omega\tau_{02}} \right] \quad (\text{S4})$$

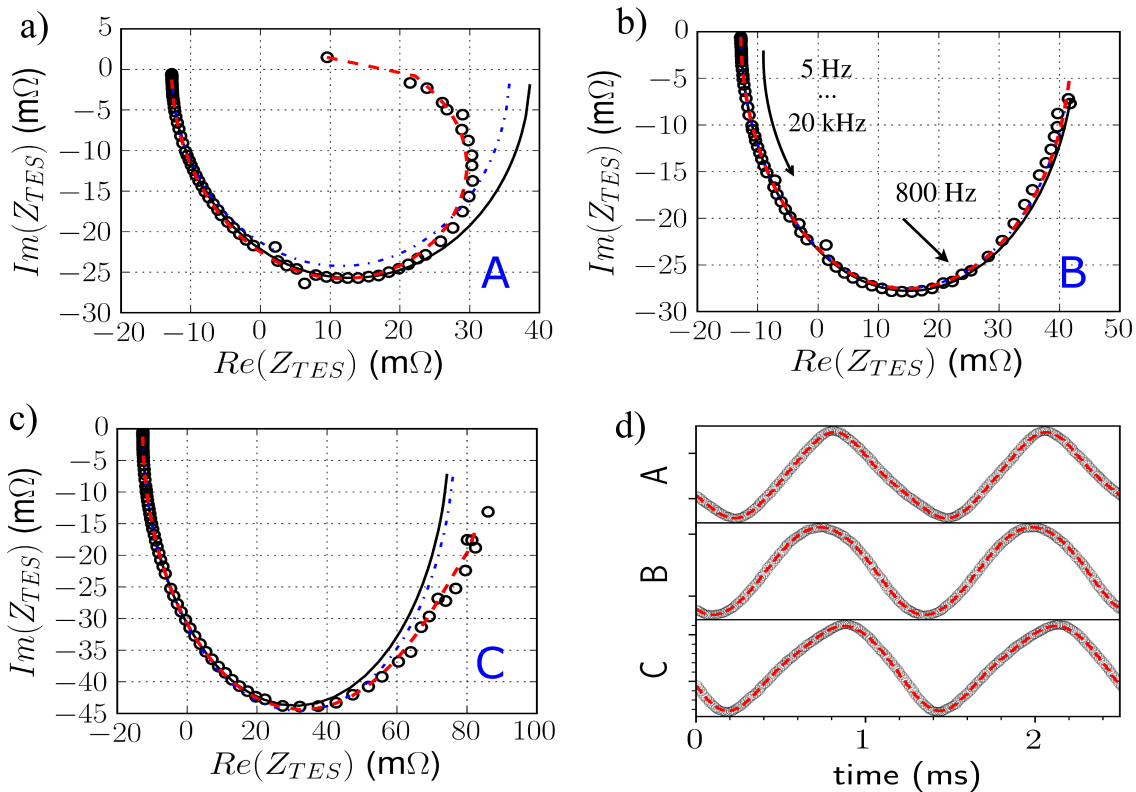


FIG. S3. (a,b,c) Complex impedance  $Z_{tes}(\omega)$  taken at the A,B and C bias points ( $R/R_N \sim 30\%$ ) shown in Fig. (S2)(a). The solid black and dash-dotted blue lines are the fit to a single and two-body thermal model, respectively. The red dashed line is the best fit with a two-body and the RSJ model. (d) Example of the detector response to a sinusoidal small excitation at 800 Hz. The red solid line is the fit to Eq. (3) in the main text. The curves have been taken with the TES operating at a bath temperature  $T_{bath} = 55$  mK

with  $\tau_{01} = C_1/(G_{bath} + G_{12})$  and  $\tau_{02} = C_2/G_{12}$  [13]. The element  $Z_{00}(\omega)$  is derived analytically in [34] using the solution for the non-linear impedance of an ac driven Josephson junction [17]. An example of the intrinsic complex impedance of the same device is shown in Fig. (S3)(a,b,c), respectively taken at the three different bias points (A,B,C) indicated in the  $I_Q - V$  (at  $R/R_N \sim 0.3$ ).

The  $Z_{tes}(\omega)$  data points are the results of a small sinusoidal excitation between 5 Hz and 20 kHz [33] away from the bias frequency of 2.5 MHz. The solid black and dash-dotted blue lines are the fit of the data, with respectively a single-body and a two-body thermal model [13, 14]. The dashed red line is the best fit with a two-body thermal model and including Eq. (S3).

As predicted in [34], we observe inward and outward inflexions of the complex impedance at high excitation frequency, which cannot be explained by a thermal effect, and are the results of the RSJ intrinsic reactance.

As an example, we show in Fig. (S3)(d) the detector response to a sinusoidal small voltage  $V_m \ll V_{ac}$  excitation at 800 Hz, when it is biased at the A,B and C points shown in Fig. (S2)(a). The red solid line is the fit to Eq. (3) in the main text. The 800 Hz frequency data point has been chosen for the example because it is typically where the response of the TES to the Johnson noise is at its maximum, for this specific bias point. The fit to Eq. (3) was done for all the frequency points, from 5 Hz up to about 20 kHz, shown in the complex impedance plots Fig. (S3)(a,b,c).



- 
- [1] K. D. Irwin and G. C. Hilton, *Cryogenic Particle Detection* (Springer-Verlag, Berlin, 2005) p. 63–149.
- [2] J. N. Ullom and D. A. Bennett, *Supercond. Sci. Technol.* **28**, 084003 (2015).
- [3] J. E. Sadleir, S. J. Smith, S. R. Bandler, J. A. Chervenak, and J. R. Clem, *Phys. Rev. Lett.* **104**, 047003 (2010).
- [4] S. J. Smith, J. Adams, C. Bailey, S. R. Bandler, J. A. Chervenak, M. Eckart, F. Finkbeiner, R. Kelley, C. Kilbourne, F. Porter, and J. Sadleir, *J. Appl. Phys.* **114**, 074513 (2013).
- [5] L. Gottardi, S. J. Smith, A. Kozorezov, H. Akamatsu, J. van der Kuur, S. R. Bandler, M. P. Bruijn, J. A. Chervenak, *et al.*, *J. Low Temp. Phys.* **193**, 209 (2018).
- [6] L. Gottardi, A. Kozorezov, H. Akamatsu, J. van der Kuur, M. P. Bruijn, R. H. den Hartog, R. Hijmering, P. Khosropanah, C. Lambert, A. J. van der Linden, M. L. Ridder, T. Suzuki, and J. R. Gao, *Appl. Phys. Lett.* **105**, 162605 (2014).
- [7] D. A. Bennett, D. S. Swetz, D. R. Schmidt, and J. N. Ullom, *Phys. Rev. B* **87**, 020508(R) (2013).
- [8] K. Irwin, *Nucl. Instrum. Methods Phys. Res., Sect., A* **559**, 718 (2006).
- [9] K. D. Irwin, *Appl. Phys. Lett.* **66**, 1998 (1995).
- [10] H. F. C. Hoevers, A. C. Bento, M. P. Bruijn, L. Gottardi, M. A. N. Korevaar, W. A. Mels, and P. A. J. de Korte, *Appl. Phys. Lett.* **77**, 4422 (2000).
- [11] Y. Takei, L. Gottardi, H. Hoevers, A. J. de Korte, J. van der Kuur, M. L. Ridder, and M. P. Bruijn, *J. Low Temp. Phys.* **151**, 161 (2008).
- [12] K. M. Kinnunen, M. R. J. Palosaari, and I. J. Maasilta, *J. Appl. Phys.* **112**, 034515 (2012).
- [13] I. J. Maasilta, *AIP Adv.* **2**, 042110 (2012).
- [14] N. A. Wakeham, J. S. Adams, S. R. Bandler, S. Beaumont, J. A. Chervenak, A. M. Datesman, M. E. Eckart, F. M. Finkbeiner, R. Hummatov, R. L. Kelley, C. A. Kilbourne, A. R. Miniussi, F. S. Porter, J. E. Sadleir, K. Sakai, S. J. Smith, and E. J. Wassell, *J. Appl. Phys.* **125**, 164503 (2019); *J. Low Temp. Phys.* **200**, 192 (2020).
- [15] See Supplemental Material for more details on the electro-thermal circuit and the derivation of the impedance and the noise equations of a TES behaving as a weak link.
- [16] C. Kirsch, L. Gottardi, M. Lorenz, T. Dauser, R. den Hartog, B. Jackson, P. Peille, S. Smith, and J. Wilms, *J. Low Temp. Phys.* **199**, 569 (2020).
- [17] W.T. Coffey, J.L. Dejardin, and Y.P. Kalmykov, *Phys. Rev. B* **62**, 3480 (2000).
- [18] J. Ullom, W. Doriese, G. Hilton, J. Beall, S. Deiker, K. Irwin, C. Reintsema, L. Vale, and Y. Xu, *Nucl. Instrum. Methods Phys. Res., Sect.* **520**, 333 (2004).
- [19] M. de Wit, L. Gottardi, E. Taralli, K. Nagayoshi, M. L. Ridder, H. Akamatsu, M. P. Bruijn, M. D’Andrea, J. van der Kuur, K. Ravensberg, D. Vaccaro, S. Visser, J. R. Gao, and J.-W. A. den Herder, *J. Appl. Phys.* **128**, 224501 (2020).
- [20] K. Likharev and V. Semenow, *Sov. Phys. JEPT Lett* **15**, 442 (1972).
- [21] S. Kogan, *Electronic Noise and Fluctuations in Solids*, 1st ed. (Cambridge University Press, USA, 2008).
- [22] A. Vystavkin, V. Gubankov, L. Kuzmin, K. Likharev, V. Migulin, and V. Semenov, *Rev. Phys. Appl.* **9**, 79 (1974).
- [23] A. Kozorezov, A. Golubov, D. Martin, P. de Korte, M. Lindeman, R. Hijmering, J. van der Kuur, H. Hoevers, L. Gottardi, M. Kupriyanov, and J. Wigmore, *J. Low Temp. Phys.* **167**, 108 (2012).
- [24] E. Lhotel, O. Coupiac, F. Lefloch, H. Courtois, and M. Sanquer, *Phys. Rev. Lett.* **99**, 117002 (2007).
- [25] A. Wessels, K. Morgan, D. T. Becker, J. D. Gard, G. C. Hilton, J. A. B. Mates, C. D. Reintsema, D. R. Schmidt, D. S. Swetz, J. N. Ullom, L. R. Vale, and D. A. Bennett, arXiv:1907.11343.
- [26] S. M. Kogan and K. Nagaev, *Zh. Eksp. Teor. Fiz* **94**, 262 (1988).
- [27] A. B. Zorin, *Physica (Amsterdam)* **108B+C**, 1293 (1981).
- [28] R. H. Koch, D. J. Van Harlingen, and J. Clarke, *Phys. Rev. B* **26**, 74 (1982).
- [29] L. G. Aslamazov and A. I. Larkin, *SJETP Lett.* **9** (1969).
- [30] K. E. Nagaev, *Sov. Phys. JETP* **67**, 579 (1988).
- [31] D. Rogovin and D. Scalapino, *Ann. Phys. (N.Y.)* **86**, 1 (1974).
- [32] M. A. Lindeman, S. Bandler, R. P. Brekosky, J. A. Chervenak, E. Figueroa-Feliciano, F. M. Finkbeiner, M. J. Li, and C. A. Kilbourne, *Rev. Sci. Instrum.* **75**, 1283 (2004).
- [33] E. Taralli, P. Khosropanah, L. Gottardi, K. Nagayoshi, M. L. Ridder, M. P. Bruijn, and J. R. Gao, *AIP Advances* **9**, 045324 (2019).
- [34] A. Kozorezov, A. A. Golubov, D. Martin, P. de Korte, M. Lindeman, R. Hijmering, J. van der Kuur, H. Hoevers, L. Gottardi, M. Kupriyanov, and J. Wigmore, *Appl. Phys. Lett.* **99**, 063503 (2011).
- [35] The internal thermal conductance in a long SNS junction is not trivial to calculate and it is likely changing along the transition. Assuming that  $G_{WF}$  depends on  $R_{\square}$  gives typically the best noise estimation over the whole transition in our TESs. The noise, in particular at low TES resistance biasing, turns out to be overestimated when  $G_{WF}$  is calculated using  $R_N$  as in Ref. [14].